Suppression of bending waves in a beam using resonators with different separation lengths ⊘

Cheng Yang; Li Cheng

Check for updates

CrossMark

View Online

Export Citation

15 February 2024 01:59:49

Suppression of bending waves in a beam using resonators with different separation lengths

Cheng Yang[a) and Li Cheng[b)

Department of Mechanical Engineering, The Hong Kong Polytechnic University, Kowloon, Hong Kong

This work is concerned with the suppression of a bending wave in a beam using resonators. Particular focus is put on the separation length between resonators. It is demonstrated that, for a beam with identical resonators attached at equal intervals, the bending wave transmission efficiency varies with respect to the separation length. The phenomena and the underlying physics are investigated by resorting to a simple beam model having two resonators resting on it. The two resonators are coupled over the segment through various bending wave components, comprising both propagating waves and evanescent waves, generated at the resonator locations where the beam encounters impedance discontinuities. The separation length, specifying the phase change of the propagating waves and the amplitude decay of the evanescent waves travelling from one resonator to the other, is thereby the parameter determining the extent to which the resonators would be coupled and the degree of the power that is transmitted. Results show, qualitatively, the difference in the working mechanism of the resonators in different separation length regions, with criteria being defined to distinguish those regions. Particularly, in the intermediate separation region, the evanescent waves are shown to play an important role in the coupling and are responsible for transmitting power, comparable with that transmitted by propagating waves, to the far field.
© 2016 Acoustical Society of America. [http://dx.doi.org/10.1121/1.4947108]

[NX]

I. INTRODUCTION

In the work of Liu *et al.*,[1] a conceptual prototype of localized resonant material was fabricated to create a band gap at the wavelength below the regime associated with the periodicity of the structure. Since then, a massive surge has been seen in the research on acoustic metamaterial, which grow along with the advancement in material design and manufacturing techniques, allowing for micro local resonant elements to be integrated to the host structures. Local resonators present in the structure generate a band gap around the frequency away from that associated with the familiar Bragg band gap, opening up the possibility of customizing a material to obtain properties that cannot be found in nature materials. An extensive review of the past work can be found in Hussein *et al.*[2]

Design of lightweight soundproof structures is of great interest for many engineering applications. The controversy is that the high stiffness-to-mass ratio of lightweight structures usually results in poor acoustic insertion loss in the frequency range controlled by the mass law. A possible solution to alleviate the problem is to embody local resonators into the structure. The creation of a vibrational stop band at low frequencies was discussed by Claeys *et al.*[3] As a common practice, the vibrational property of a structure, with attached local resonators, is characterized by the dispersion curve, which, in view of the periodic distribution of local resonators, could be resolved by confining the analysis into a unit element. Any suitable technique for modeling periodic structures could be employed for this purpose. For example, the dynamic stiffness matrix of a structure segment extracted from the finite element (FE) modeling could be post-processed, with periodic conditions and proper force equilibrium relations imposed on the boundaries of the segment, to obtain the dispersion curve of the whole periodic structure.[4–7]

The key feature of an acoustic metamaterial is the existence of the band gap brought about by the local resonance mechanism, which has long been utilized for vibration suppressions.[8–13] The effect of a one degree of freedom (DoF) resonator (dynamic vibration absorber) on the vibration of a beam was examined in the work of Brennan,[14] in which the tuning of the resonator for maximum wave attenuation was investigated. A mathematical expression was also given to approximately describe the relationship between the resonator mass and the optimal tuning frequency. The work was then extended to a two DoF case,[15] with emphasis on the effects of different resonator configurations. Upon encountering a resonator, a travelling bending wave in the beam is scattered, generating propagating waves and evanescent waves. The former is capable of reaching the far field while the latter is confined within the near field. The influences of these two wave components were investigated by El-Khatib *et al.*[16,17] in two scenarios, where a resonator was placed either in the near or far fields of a point excitation, and the

---

[a)Present address: Department of Mechanical and Aerospace Engineering, The Hong Kong University of Science and Technology, Hong Kong Special Administrative Region.
[b)Electronic mail: li.cheng@polyu.edu.hk

tuning frequency for maximum transmission reduction was sought in different scenarios. It is relevant to note that the above four papers all consider one single resonator. The reduction of bending wave motion in a beam by multiple resonators was reported by Thompson,[18] where the resonators were approximated as a continuous resonant medium attached to the beam. A more explicit investigation was carried out by Gao et al.,[19] in which, each resonator was modeled as an impedance discontinuity at the point of attachment. The effects of various parameters (such as resonator mass and separation lengths between resonators) on the minimum transmission efficiency, the effective bandwidth and the amount of the reduction over the effective bandwidth were examined in a quantitative manner. The work allows the observation of some interesting phenomena. For example, the wave suppression effect is less sensitive to the number of resonators when the separation lengths are small as opposed to the case with larger separation length. The occurrence of those phenomena, however, is not explained. The lack of the physical understanding of and the explanation to those issues motivates the present work. In particular, our interest is to explore how resonators with different separation lengths interact with each other from the wave propagation viewpoint, as well as the role played by the propagating and evanescent waves in the process of power transmission. It is intuitive to surmise that the interaction among resonators would depend greatly on the separation length. For sparse configuration with larger separation, the propagating waves should dominate the interaction; whilst for shorter length, evanescent waves could be a significant player. In particular, a single evanescent wave, incapable of transmitting energy to the far field, might be involved in power transmission process through the interaction with another evanescent wave travelling in the opposite direction.[16,17] This suggests that, in the presence of multiple resonators, the evanescent waves would play different roles in determining the effect of the resonators for different separation lengths. Another point of motivation is the inclination to understand the interaction of local resonators in acoustic metamaterial, which is somehow overlooked by the global dispersion curve derived from the local structural unit based on structural periodicity. A well-understood working principle of the resonators would benefit the structural design for various vibration control applications.

The paper is organized as follows: Sec. II establishes a general model for the bending wave propagation in a beam with an attached resonator array. Section III illustrates the control mechanism of the bending wave with one resonator. The cases for two resonators at different intervals are investigated in Sec. IV. The underlying physics are revealed and explained. Section V studies the role of evanescent waves in the power transmission process. Conclusions are then drawn in Sec. VI.

II. MODEL DEVELOPMENT

A. Wave propagation in a beam with one resonator

The structure under investigation is a Euler–Bernoulli beam of infinite length, shown in Fig. 1. Ignoring the effects of in-plane shear stiffness and rotary inertia, the general
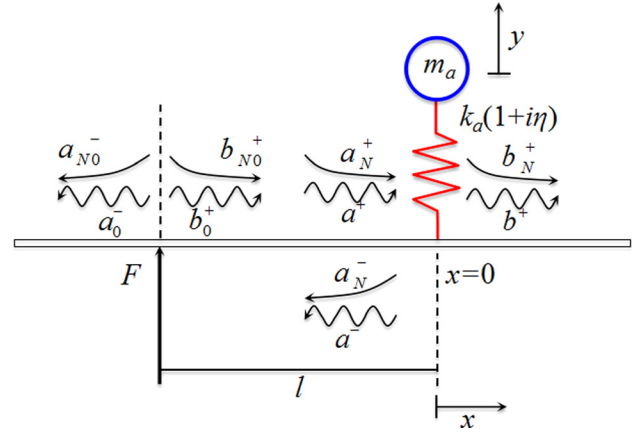

FIG. 1. (Color online) A diagram showing the wave components for a beam with a single resonator.

wave motion in terms of transverse flexural displacement, w, is expressed as[20]

$$w(x,t) = (Ae^{-jk_bx} + Be^{jk_bx} + Ce^{-k_bx} + De^{k_bx})e^{j\omega t}. \quad (1)$$

It is clearly shown in Eq. (1), that the wave motion in the beam consists of four wave components: the first two are the propagating waves with a phase speed $c_b = \omega/k_b$, where $k_b = (\omega^2 m/EI)^{1/4}$ is the bending wavenumber, in which m and EI are, respectively, the mass per unit length and the bending stiffness of the beam; whilst the last two are the evanescent waves, the amplitudes of which decay exponentially with distance x. Evanescent waves contribute little to the far field vibrational displacement, whilst in the near field, their influence may be substantial. In Eq. (1), the sign in front of the wavenumber indicates the positive-going $(-)$ and negative-going $(+)$ waves, respectively.

Following the notation in Fig. 1, Eq. (1) can be rewritten for the region $x < 0$ as

$$w(x) = a^+ e^{-jk_bx} + a^- e^{-jk_bx} + a_N^+ e^{-k_bx} + a_N^- e^{-k_bx}, \quad (2)$$

and for $x > 0$ as

$$w(x) = b^+ e^{-jk_bx} + b_N^+ e^{-k_bx}. \quad (3)$$

The time dependence is well understood and will be omitted hereafter for simplicity. Across the attach point of the resonator $x = 0$, the transverse displacement, i.e., $w(0)$, is continuous, giving

$$a^+ + a_N^+ + a^- + a_N^- = b^+ + b_N^+. \quad (4)$$

Similarly, the continuity of the angular displacement yields

$$-ja^+ - a_N^+ + ja^- + a_N^- = -jb^+ - b_N^+. \quad (5)$$

Shear force equilibrium is also satisfied at the point, thus

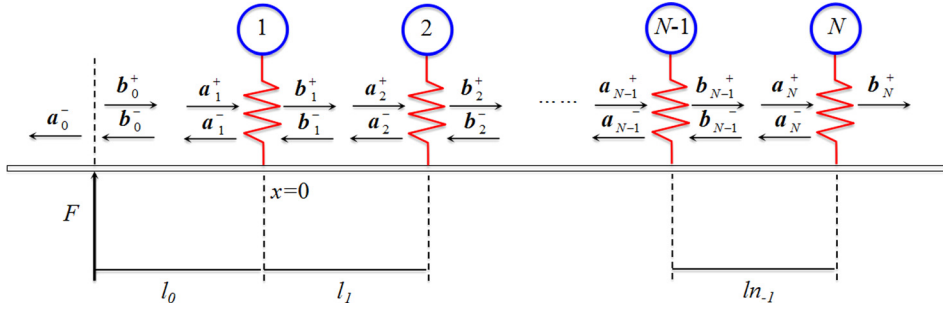$$EIk_b^3(ja^+ - a_N^+ - ja^- + a_N^- - jb^+ + b_N^+) - k_{eq}w(0) = 0, \quad (6)$$

Cheng Yang and Li Cheng

FIG. 2. (Color online) A diagram showing a beam with multiple resonators.

where k_{eq} is the equivalent dynamic stiffness of the resonator, expressed by[18]

$$k_{eq} = \frac{\omega^2 k_a(1 + j\eta)}{\omega^2 - \omega_a^2(1 + j\eta)}, \qquad (7)$$

in which $\omega_a = (k_a/m_a)^{1/2}$ is the natural frequency of the resonator itself, with k_a, m_a, and η being, respectively, its stiffness, mass, and loss factor.

For a resonator with single DoF, which only exerts transverse force upon the beam, the bending moment equilibrium at $x = 0$ is expressed as

$$-a^+ + a_N^+ - a^- + a_N^- + jb^+ - b_N^+ = 0. \qquad (8)$$

The coefficients of the different wave components can be conveniently rearranged in vectors as

$$\boldsymbol{a}^+ = \begin{bmatrix} a^+ \\ a_N^+ \end{bmatrix}, \quad \boldsymbol{a}^- = \begin{bmatrix} a^- \\ a_N^- \end{bmatrix}, \quad \boldsymbol{b}^+ = \begin{bmatrix} b^+ \\ b_N^+ \end{bmatrix}. \qquad (9)$$

The relationships among these coefficients are established as

$$\boldsymbol{b}^+ = \boldsymbol{T}\boldsymbol{a}^+, \quad \boldsymbol{a}^- = \boldsymbol{R}\boldsymbol{a}^+, \qquad (10)$$

in which, the 2×2 $\boldsymbol{T}$ and $\boldsymbol{R}$ matrices are the transmission and reflection matrices describing the contribution of the propagating and the evanescent wave components of the incident wave in constructing the corresponding wave components in the transmitted and reflected waves.

With the notation defined in Eq. (9), Eqs. (4)–(6) and (8) can be written in a matrix form as

$$\begin{bmatrix} 1 & 1 & 1 & 1 \\ -j & -1 & j & 1 \\ j & -1 & -j & 1 \\ -1 & 1 & -1 & 1 \end{bmatrix} \begin{bmatrix} \boldsymbol{a}^+ \\ \boldsymbol{a}^- \end{bmatrix} = \begin{bmatrix} 1 & 1 \\ -j & -1 \\ j+\varepsilon & -1+\varepsilon \\ -1 & 1 \end{bmatrix} \boldsymbol{b}^+, \qquad (11)$$

where

$$\varepsilon = \frac{k_{eq}}{EIk_b^3} = \frac{\psi(1 + j\eta)}{\Omega^2 - 1 - j\eta}, \qquad (12)$$

with $\Omega = \omega/\omega_a$ being the non-dimensional frequency, and ψ the non-dimensional mass ratio defined as

$$\psi = \frac{2\pi m_a}{\lambda m}, \qquad (13)$$

where λ is the wavelength. $\boldsymbol{T}$ and $\boldsymbol{R}$ matrices can then be sought by using the relations defined in Eq. (10).

Given a transverse excitation force on the beam at a distance l to the left of the resonator, the coefficients of the positive-going wave components are[21]

$$\boldsymbol{b}_0^+ = \begin{bmatrix} b_0^+ \\ b_{N0}^+ \end{bmatrix} = -\frac{F}{4EIk_b^3} \begin{bmatrix} i \\ 1 \end{bmatrix}. \qquad (14)$$

For the incident wave at $x = 0$, after travelling over a distance l from the point where the force is imposed,

$$\boldsymbol{a}^+ = \boldsymbol{Z}\boldsymbol{b}_0^+, \qquad (15)$$

where

$$\boldsymbol{Z} = \begin{bmatrix} e^{-ik_b l} & 0 \\ 0 & e^{-k_b l} \end{bmatrix}. \qquad (16)$$

$\boldsymbol{Z}$ is the transfer matrix characterizing the phase change of the propagating wave component and the amplitude decay of the evanescent wave component over the distance l. By substituting Eqs. (14)–(16) into the determined $\boldsymbol{T}$ and $\boldsymbol{R}$, the wave motion in the beam can be known explicitly.

B. Wave propagation in a beam with multiple resonators

For a beam with multiple resonators, the transmission and reflection matrices could be obtained in a recursive manner. Considering the configuration shown in Fig. 2, a beam with an array of N resonators is excited by a transverse force at $x = -l_0$. At the point where the Nth resonator is located, the incident, reflected and transmitted waves are related by

$$\boldsymbol{a}_N^- = \boldsymbol{R}_N\boldsymbol{a}_N^+, \quad \boldsymbol{b}_N^+ = \boldsymbol{T}_N\boldsymbol{a}_N^+, \qquad (17)$$

and those at the point where the $(N-1)$th resonator is located are related by

$$\begin{aligned} \boldsymbol{a}_{N-1}^- &= \boldsymbol{T}_{N-1}\boldsymbol{b}_{N-1}^- + \boldsymbol{R}_{N-1}\boldsymbol{a}_{N-1}^+, \\ \boldsymbol{b}_{N-1}^+ &= \boldsymbol{T}_{N-1}\boldsymbol{a}_{N-1}^+ + \boldsymbol{R}_{N-1}\boldsymbol{b}_{N-1}^-. \end{aligned} \qquad (18)$$

The transfer relations for the waves between the $(N-1)$th and the Nth resonators are

$$\boldsymbol{a}_N^+ = \boldsymbol{Z}_{N-1}\boldsymbol{b}_{N-1}^+, \quad \boldsymbol{b}_{N-1}^- = \boldsymbol{Z}_{N-1}\boldsymbol{a}_N^-, \qquad (19)$$

where

$$\mathbf{Z_{N-1}} = \begin{bmatrix} e^{-ik_b l_{N-1}} & 0 \\ 0 & e^{-k_b l_{N-1}} \end{bmatrix} \quad (20)$$

is the matrix evaluating the transfer relation for the waves travelling over distance l_{N-1} between the $(N-1)$th and the Nth resonators. The positive-going wave incident at the $(N-1)$th resonator is related to the reflected wave at the $(N-1)$th resonator and the wave transmitted over the Nth resonator by

$$\mathbf{a}_{N-1}^{-} = \mathbf{R}_{N-1N-1}\mathbf{a}_{N-1}^{+}, \quad \mathbf{b}_{N}^{+} = \mathbf{T}_{N-1N}\mathbf{a}_{N-1}^{+}. \quad (21)$$

Combining Eqs. (17)–(21) yields

$$\mathbf{T}_{N-1N} = \mathbf{T}_N(\mathbf{I} - \mathbf{Z}_{N-1}\mathbf{R}_{N-1}\mathbf{Z}_{N-1}\mathbf{R}_N)^{-1}\mathbf{Z}_{N-1}\mathbf{T}_{N-1}, \quad (22)$$

and

$$\mathbf{R}_{N-1N-1} = \mathbf{R}_{N-1} + \mathbf{T}_{N-1}(\mathbf{I} - \mathbf{Z}_{N-1}\mathbf{R}_N\mathbf{Z}_{N-1}\mathbf{R}_N)^{-1}$$
$$\times \mathbf{Z}_{N-1}\mathbf{R}_N\mathbf{Z}_{N-1}\mathbf{T}_{N-1}. \quad (23)$$

In the above equations, the single subscript of $\mathbf{T}$ and $\mathbf{R}$ denotes the transmission and reflection coefficients for individual resonator, while the double indexed ones represent those for the resonators consisting of the $(N-1)$th and the Nth resonators.

The obtained $\mathbf{T}_{N-1N}$ and $\mathbf{R}_{N-1N-1}$ can be used to obtain $\mathbf{T}_N$ and $\mathbf{R}_N$ in a recursive way, respectively, in Eqs. (22) and (23), to get the transmission and reflection matrices of the resonator group comprising the $(N-2)$th, $(N-1)$th, and Nth resonators (derivation is made by changing the subscript $N-1$ to $N-2$). The transmission and reflection coefficients of the entire resonator array are then obtained by repeating the above process. This leads to the coefficients of the wave components of the transmitted wave as

$$\mathbf{b}_N^{+} = \mathbf{T}_{1N}\mathbf{a}_1^{+} = \mathbf{T}_{1N}\mathbf{Z}_0\mathbf{b}_0^{+}. \quad (24)$$

Equation (24) can be substituted into Eq. (17) to get the wave components incident and reflected at the Nth resonator, i.e., $\mathbf{a}_N^{+}$ and $\mathbf{a}_N^{-}$, and those at the $N-1$th resonator can be derived from Eqs. (18) and (19)

$$\mathbf{a}_{N-1}^{+} = \mathbf{T}_{N-1}^{-1}(\mathbf{Z}_{N-1}^{-1}\mathbf{a}_N^{+} - \mathbf{R}_{N-1}\mathbf{Z}_{N-1}\mathbf{a}_N^{-}), \quad (25)$$

and

$$\mathbf{a}_{N-1}^{-} = \mathbf{R}_{N-1}\mathbf{a}_{N-1}^{+} + \mathbf{T}_{N-1}\mathbf{Z}_{N-1}\mathbf{a}_N^{-}. \quad (26)$$

The coefficients of the incident and reflected wave components at any resonator location can therefore be obtained in a recursive manner. To quantify the energy transmission process, a transmission efficiency, which quantifies the power transmitted through N resonators to the far field, is defined as

$$\tau = 10\log_{10}\left|\frac{b_N^{+}}{a_0^{+}}\right|^2. \quad (27)$$

III. BENCHMARK CASE WITH SINGLE RESONATOR

Control of the bending wave motion in a beam with a single resonator is first addressed to understand the

mechanism of the interaction between the resonator and the beam on one hand, and to develop the benchmark for subsequent analyses on the other hand. To avoid the near field effect caused by the point force excitation, the resonator is located far away from the force, with a non-dimensional length $k_n l_0 = 10$. The same mass ratio and loss factor of the resonator, i.e., $\psi_n = 0.5$, $\eta = 0.001$, as those in Ref. 19, are used in the calculation. The subscript n denotes the quantity evaluated at the resonance frequency of the resonator ($\omega = \omega_a$).

The transmission efficiency for the current case is shown in Fig. 3. It can be observed that the minimum transmission occurs at the frequency away from the resonance frequency of the resonator where the transmission is reduced by 3 dB only. This indicates that the resonator should be properly tuned for maximum vibration reduction.

The time-averaged power flow in a beam undergoing bending motion can be expressed as[22]

$$\overline{P(x)} = -\overline{M\dot{\theta}} - \overline{Qv}, \quad (28)$$

where the bar denotes time average. An explicit expression of Eq. (28) is given in the Appendix. The right-hand side terms of Eq. (28) show the two components of the overall power flow through the bending moment and the shear force, respectively.

With Eq. (28), the non-dimensionalized power (with respect to the injected power of the force excitation) for the two components is plotted in Figs. 4(a) and 4(b), respectively. It can be seen that, at the non-dimensional frequency $\Omega = 1$, the power associated with the shear force is zero, while that associated with the bending moment is 0.5. This suggests that at this frequency, the resonator exerts a transverse force upon the beam to pin the structure at the point of attachment, preventing the transmission of power through shear force. Therefore, the total power is only transmitted through bending moment and is half of that injected by the force excitation, in agreement with the 3 dB reduction in the transmission curve in Fig. 3.
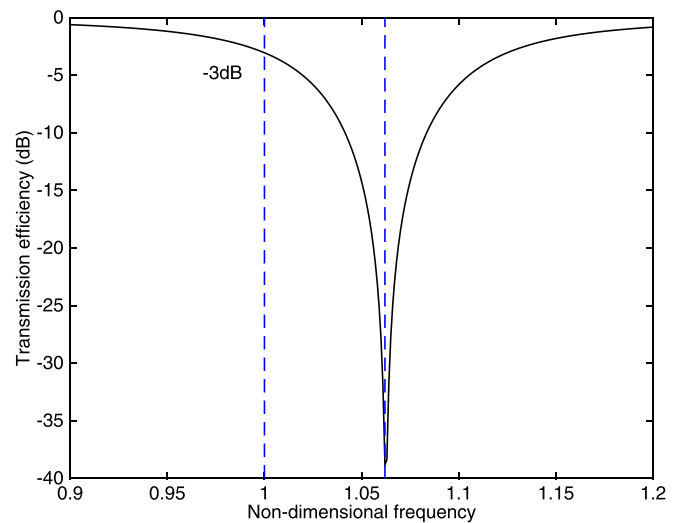

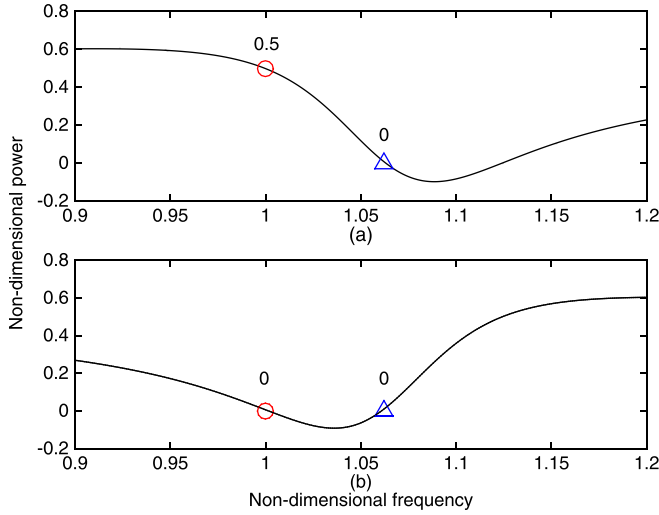FIG. 3. (Color online) Transmission efficiency for a beam with a single resonator.

FIG. 4. (Color online) Non-dimensional power of the power flow component for the beam with a single resonator. (a) Component associated with the bending moment calculated by Eq. (A4); (b) component associated with shear force calculated by Eq. (A5).

At the transmission dip, however, both power flow components are zero, indicating a quasi-termination of the power transmission. The vibration of the structure in this case is dominated by the resonator and the upstream part of the beam. The corresponding frequency, i.e., Ω_t, can be estimated by the following expressions given by Brennan[14]

$$\Omega_t^2 = 1 + \frac{\psi_n}{4}\Omega_t^{1/2}, \qquad (29)$$

where Ω_t is called tuned frequency. Numerical calculations show that Ω_t increases with ψ_n. This is understandable in that the equivalent dynamic stiffness of the resonator, expressed by Eq. (7), is proportional to the stiffness of the resonator. When the resonator mass is increased, its stiffness should be increased concurrently to keep the same ω_a, leading to an increase in the equivalent dynamic stiffness as well as Ω_t. It follows that, for a beam subject to an excitation at a fixed frequency, a resonator with larger mass should be detuned to a larger extent from the excitation frequency.

IV. TWO RESONATORS WITH DIFFERENT SEPARATION LENGTHS

This section investigates the influence of the separation length between resonators on the suppression of wave motion in the beam. Two identical resonators, with mass equal to $m_a/2$ each, are separated by a non-dimensional length $k_n l$, with l being the distance between them. Other parameters remain the same as those used in Sec. III.

Figure 5 shows the transmission efficiency (τ) against frequency for different $k_n l$ values. It is obvious that, despite the same resonators being used, the power transmission is quite different and evolves in a complex manner with respect to $k_n l$. For small separation length ($k_n l = 0.01$), only one single transmission dip is noticeable in the curve. When the length is increased ($k_n l = 0.1$ and 0.5), an extra dip appears at $\Omega = 1$. Further increasing the length ($k_n l = 1$) would shift
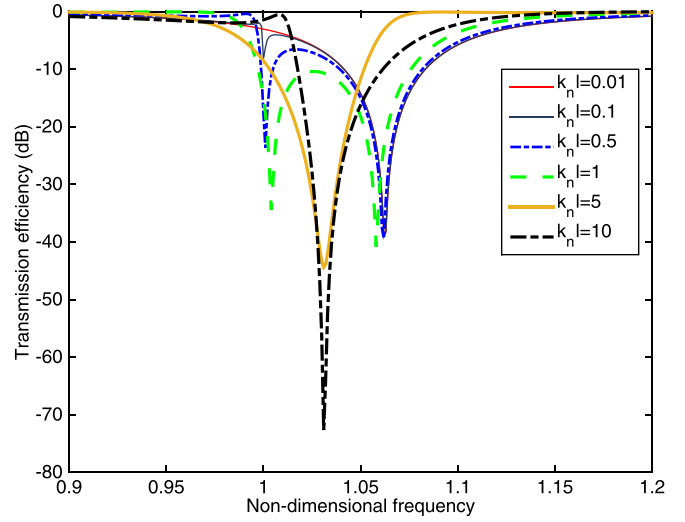

FIG. 5. (Color online) Transmission efficiencies for the beam with two resonators separated by different non-dimensional lengths $k_n l$.

the two dips towards each other, before they finally merge together to form a more pronounced dip for even larger separation ($k_n l = 5$). Further increasing the separation length ($k_n l = 10$) only gives rise to a change in amplitude with no further shift in the frequency of the merged transmission dip. These observed phenomena are discussed and explained in detail in Secs. IV A–IV C.

A. Small separation length (Zone I)

The case of small separation length ($k_n l = 0.01$) is first investigated. Recalling the four wave components in the general solution of the governing equation: A pair of propagating and evanescent waves travelling in the positive direction and another pair travelling in the negative direction, a superposition of them gives the overall response of the beam. In particular, the responses at the points of attachments are related by Eqs. (19) and (20), which describe the phase change of the propagating waves and the amplitude decay of the evanescent waves, over the distance between the resonators.

Figure 6 depicts the non-dimensionalized displacement amplitude (normalized by $-F/4EIk_b^3$) of the four wave components and that of the resultant wave motion, at Ω_t, over the distance between the two resonators. It can be seen that, the four wave components, by virtue of the closeness of the resonators, are basically constant over the segment, indicating no change in either the phase of the propagating waves or the amplitude of the evanescent waves within such a small separation length. Therefore, two resonators placed in the immediate vicinity of each other would be equivalent to a single resonator having the same total equivalent mass. This is evidenced in Fig. 7, in which, the transmission efficiency for the case with two resonators overlaps with that with a single resonator but doubled mass.

B. Intermediate separation length (Zone II)

When the separation length is increased, to $k_n l = 0.1$ for example, an extra transmission dip appears (Fig. 5) at

J. Acoust. Soc. Am. **139** (5), May 2016

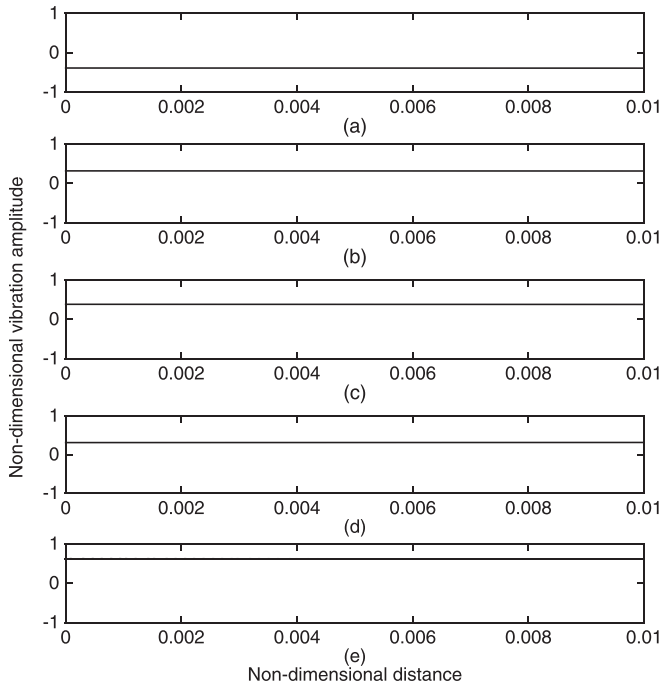Cheng Yang and Li Cheng   2365

FIG. 6. Non-dimensional displacement amplitudes for the wave components and the resultant motion, of the beam spanning from the first resonator (left end) to the second resonator (right end), at the transmission dip ($\Omega = 1.062$). (a) Positive-going propagating wave; (b) positive-going evanescent wave; (c) negative-going propagating wave; (d) negative-going evanescent wave; (e) resultant wave motion.

FIG. 8. (Color online) Non-dimensional displacement amplitude for the resultant motion of the beam spanning from the first resonator (left end) to the second resonator (right end), at the two transmission dips ($\Omega = 1$ and $\Omega = 1.062$).

$\Omega = 1$, while the original transmission dip remains at Ω_t. To understand the underlying mechanism, it is relevant to have a closer examination of the beam segment between the two resonators, at the frequencies of the transmission dips. The non-dimensionalized displacement amplitude of the segment is depicted in Fig. 8. At Ω_t, the beam segment experiences a large vibration as a result of the strong coupling between the two resonators through the beam, leading to the vanishing of power flow in the beam. To substantiate this argument, the

power flow components, associated with the bending moment and the shear force, are plotted against frequency in Fig. 9. Similar as the one resonator case, both power components are zero. This, however, is different to what happens at $\Omega = 1$, where the vibration of the beam segment is significantly smaller than that at Ω_t, as shown in Fig. 8. At $\Omega = 1$, the resonators impose strong constraint at the points of attachments. However, different from the single resonator case, in which the beam structure is completely pinned, the beam still undergoes modest vibration as shown in Fig. 8, due to changes in the coupling between the resonators. For a separation length in this region, both propagating and evanescent waves serve as an agent for power transmission. Over the segment, the variation of the propagating and evanescent waves would cause different responses of the resonators and affect the coupling between them. The transversal constraint
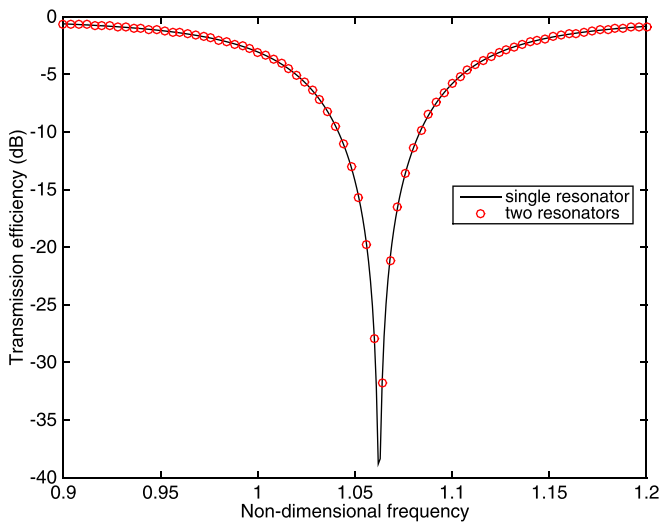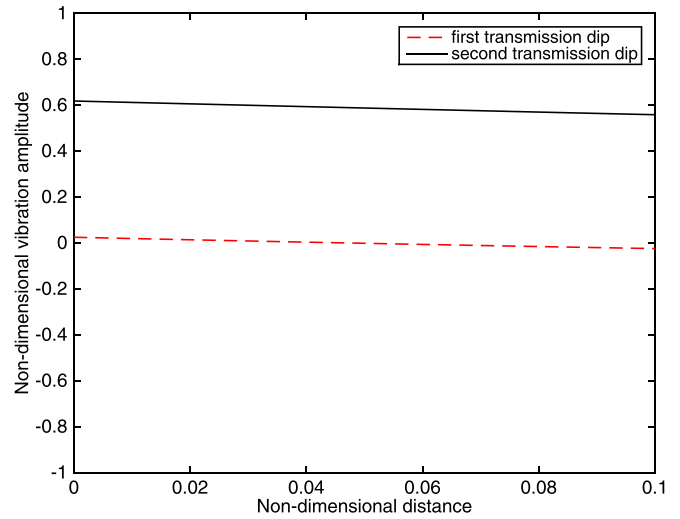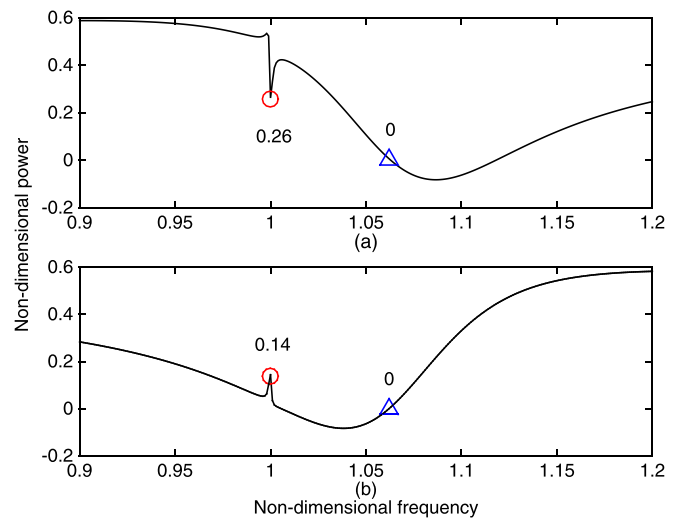

FIG. 7. (Color online) Comparison of the transmission efficiencies for two resonators, and a single resonator with the mass equal to the sum of the mass of the two individual resonators. All resonators have identical resonance frequency and loss factor.

FIG. 9. (Color online) Non-dimensional power of the power flow component for the beam with two resonators separated by $k_n l = 0.1$. (a) The component associated with bending moment calculated by Eq. (A4); (b) the component associated with shear force calculated by Eq. (A5).

at the ends of the beam segment is then partially released and the pinning effect becomes less obvious than that in the one resonator case. This changed coupling can be further observed by checking the power flow components at $\Omega = 1$ in Fig. 9, where the power associated with the bending moment decreases to 0.26 (from 0.5) and that associated with the shear force increases to 0.14 (from 0), compared with the single resonator case.

It follows that increasing the separation length would modify the way in which the resonators are coupled over the beam segment, and consequently affect the power that could be transmitted. Figure 10 depicts the non-dimensional power associated with the bending moment, at $\Omega = 1$, as a function of $k_n l$. It can be seen that the curve starts from a value asymptotic to half of the total power injected to the beam, corresponding to the case of small separation length. The curve decreases with the increase of the separation length, indicating a reduced power transmission through bending moment. A threshold separation length can then be defined to distinguish the so-called small and intermediate separation regions. This is taken as $k_n l$ equals 0.105, at which the power component associated with the bending moment is half of that for the single resonator case, i.e., non-dimensional power being 0.25. Below this value, the two resonators can be regarded as a combined resonator, generating one single power transmission dip.

When the separation length is further increased, as shown in Fig. 5, the transmission efficiency at the two dips is found not only to decrease in value but also to shift in frequency towards each other. The shift phenomenon can be visualized, by plotting the frequencies of the two transmission dips against the separation length, in Fig. 11. The figure shows that the two dips, which arise initially at fixed frequencies, converge with the increase of separation length until merging at $k_n l \approx \pi$, after which only one transmission dip exists. Note this value corresponds to a physical separation length of half wavelength of the bending wave. With

FIG. 11. (Color online) Frequencies of the two transmission dips as a function of the non-dimensional length $k_n l$ between the two resonators. The vertical line distinguishes Zone I and Zone II.

this, the second threshold, i.e., $k_n l \approx \pi$, can be defined to distinguish the intermediate separation region from the large separation region.

For $k_n l$ falling in the intermediate separation region bounded by the two threshold values ($k_n l \approx 0.105$ and $k_n l \approx \pi$), the two resonators are coupled over the beam segment in terms of the propagating waves and appreciable evanescent waves and cause two power transmission dips in the spectrum.

It is interesting to explore the reason that leads to the merging of the two power transmission dips. This can be done by observing the displacement amplitude of the resultant wave motion of the beam segment at the frequency of the merged dip, for separation length $k_n l = \pi$. The result is given in Fig. 12, where a large vibration is found near the first resonator (upstream), while a small vibration near the second resonator (downstream). This difference in vibration level indicates the different roles of the two resonators in the resonator-beam system: The first resonator couples with the
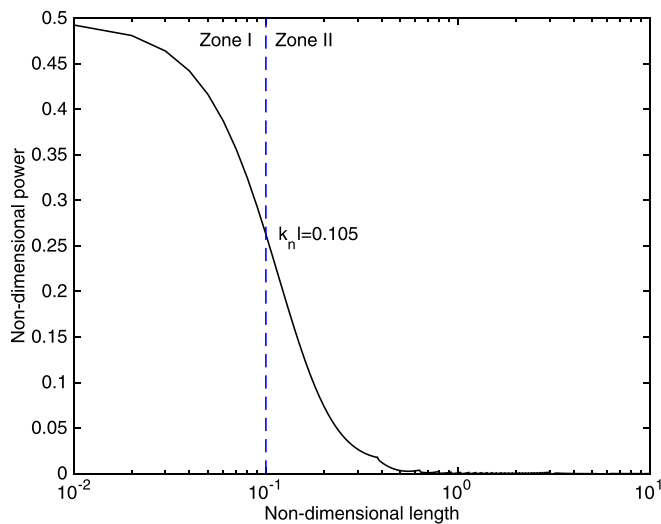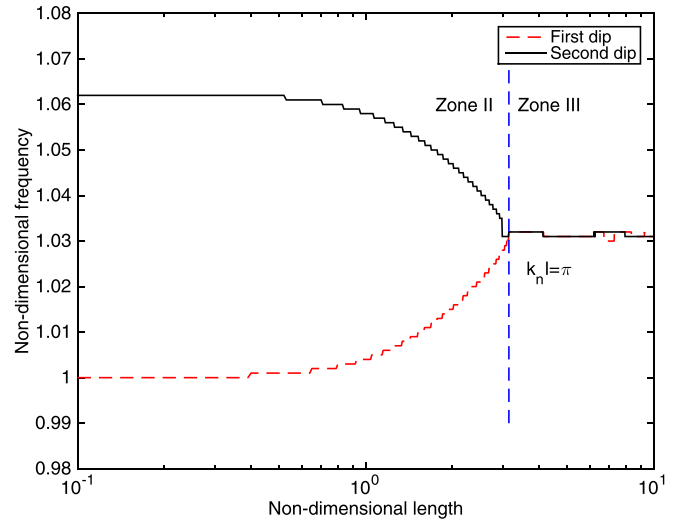

FIG. 10. (Color online) Non-dimensional power flow component, associated with the bending moment at the frequency of the first transmission dip, as a function of the non-dimensional length $k_n l$ between the two resonators. The vertical line distinguishes Zone I and Zone II.
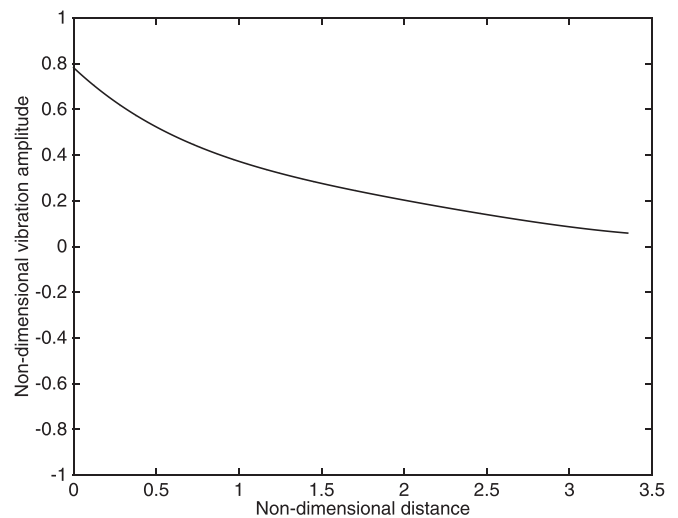

FIG. 12. Non-dimensional displacement amplitude for the resultant motion of the beam spanning from the first resonator (left end) to the second resonator (right end), at the transmission dip ($\Omega = 1.032$), when $k_n l = \pi$.

J. Acoust. Soc. Am. **139** (5), May 2016
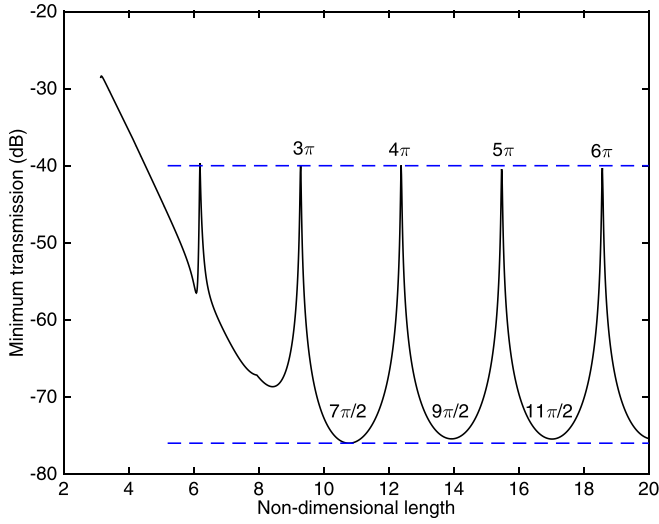
Cheng Yang and Li Cheng   2367

FIG. 13. (Color online) Minimum power transmissions as a function of the non-dimensional length between the two resonators. The calculation is made for separation length in Zone III.

beam segment to introduce a bending constraint, while the second resonator pins the structure. This could also be manifested, implicitly, by substituting the resonance frequency into Eq. (29). A simple calculation shows that the effective mass in the system, for such separation length, equals half of the overall physical mass of the resonators, i.e., the mass of the first resonator. This is in agreement with the above explanation where the second resonator pins the structure and does not introduce additional mass into the coupled system.

C. Large separation length (Zone III)

After the second threshold value, increasing separation length would result in only one transmission dip in the power transmission curve, and the amplitude of the transmission dip varies with respect to the separation length. This can be visualized by plotting the minimum transmission efficiency against the separation length in Fig. 13. As can be seen, the minimum transmission oscillates within a bounded region,

where the upper bound occurs when $k_n l = n\pi$ and the lower bound occurs when $k_n l = (n + 1/2)\pi$, where n is an integer larger than 1. For large separation length, the influence of the evanescent waves is weak in the coupling, and the two resonators are merely coupled through propagating waves. The separation length, which specifies the phase changes of the propagating waves over the beam segment, thereby determines the amount of the power that could be transmitted.

V. THE ROLE OF EVANESCENT WAVES IN THE PRESENCE OF MULTIPLE RESONATORS

The dependence of the coupling between resonators on the separation length suggests the importance of the evanescent waves in determining the power transmission in the beam. To explore the underlying physics, the role of evanescent waves is studied in two cases where a resonator array comprising five and 10 resonators is used, respectively. The case of two resonators will be taken as a reference for comparison. For all configurations, the overall mass of the resonators is maintained a constant and the mass is equally allocated to individual resonators. All resonators are therefore set to have identical resonance frequency and loss factor, attached at equal interval.

Figure 14 depicts the power transmission efficiencies for two, five, and 10 resonators with different separation lengths, corresponding to the three zones defined in Sec. IV. Obviously, the power transmission curve is independent of resonator number for small separation [$k_n l = 0.01$, Zone I, Fig. 14(a)]. When $k_n l$ is increased to 1 (Zone II), the propagating waves and evanescent waves interfere with each other, giving rise to multiple transmission dips [Fig. 14(b)], before they all merge to a deeper dip when $k_n l = 10$ [Zone III, Fig. 14(c)], where the propagating waves dominate the coupling between resonators. The phenomenon is basically identical to the two resonator cases, except for that in the intermediate separation case, where multiple dips appear in the presence of multiple resonators, and the larger the resonator number is, the earlier the merging of these dips takes place.
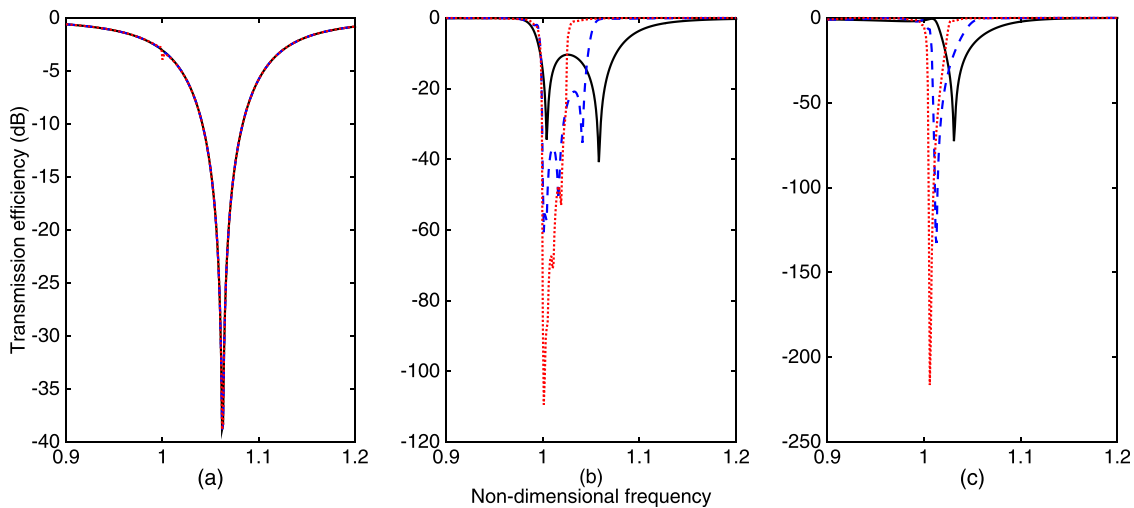

FIG. 14. (Color online) Transmission efficiencies for the beam with different number of resonators separated in different separation lengths $k_n l$. (a) $k_n l = 0.01$ (Zone I); (b) $k_n l = 1$ (Zone II); (c) $k_n l = 10$ (Zone III). ———— 2 resonators; - - - - - - - 5 resonators; - - - - - - - - - - 10 resonators.

Generally speaking, increasing the number of resonators helps reduce the power transmission, except for very small separation lengths. This is in agreement with the conclusion drawn in the two resonators case.

The aforementioned phenomenon can be explained by investigating the power transmitted by various wave components, especially the evanescent waves, in the three zones. It is shown that, an evanescent wave, which holds energy in the near field, may be able to transmit energy to the far field through the interaction with another evanescent wave traveling in the opposite direction. This is evidenced by the location independent term $|a_N^+||a_N^-|\sin(\phi_4 - \phi_2)$ in the time-averaged power flow expression, i.e., Eq. (A6) in the Appendix. It is reasonable to surmise that, in the intermediate separation length region (Zone II), the role of evanescent waves might be substantial. This is investigated by the far field power transmitted, respectively, by the propagating waves, i.e., $|a^+|^2 + |a^-|^2$, and the evanescent waves, i.e., $|a_N^+||a_N^-|\sin(\phi_4 - \phi_2)$, for the three cases in Fig. 15. For the two resonators case, it shows that, in general, the power is carried mainly by the propagating waves, especially for small and large separation lengths (Zones I and III). In the intermediate separation region (Zone II), Fig. 15(b) shows two interesting phenomena: First, evanescent waves are more noticeable, within the frequency region where the resonators are effective (Ω from 1 to 1.1), and carry appreciable power compared with that by the propagating waves; second,

the power transmitted downstream of the beam is partially reverted back to the upstream part of the beam by the evanescent waves below the resonance frequency of the resonators, as evidenced by the negative value of the non-dimensional power. This underlines the role of evanescent waves in the power transmission process and explains the reason behind the complex power transmission phenomena observed in intermediate separation length region reported in Sec. IV B.

The effect of resonator number is shown in Figs. 15(d)–15(i). Due to the increase of the resonator number, the so-called stop band starts to appear. Again the dominance of the propagating waves in both cases is obvious. It is relevant to note, however, due to the fact that the total mass of the resonator array is kept constant in the current simulation, the mass of an individual resonator would reduce with the increase of resonator number. In this connection, the near field effect due to the evanescent waves is less obvious. This treatment arises from the concern in practical problems where the extra weight introduced by the control devices should be as small as possible. If, however, the total added mass of the system is not a concern, the mass of each resonator can then be kept the same when the resonator number increases. Numerical results show that the width of the stop band and effect of the evanescent waves, as discussed in the two resonators case, should remain the same or even enhanced.
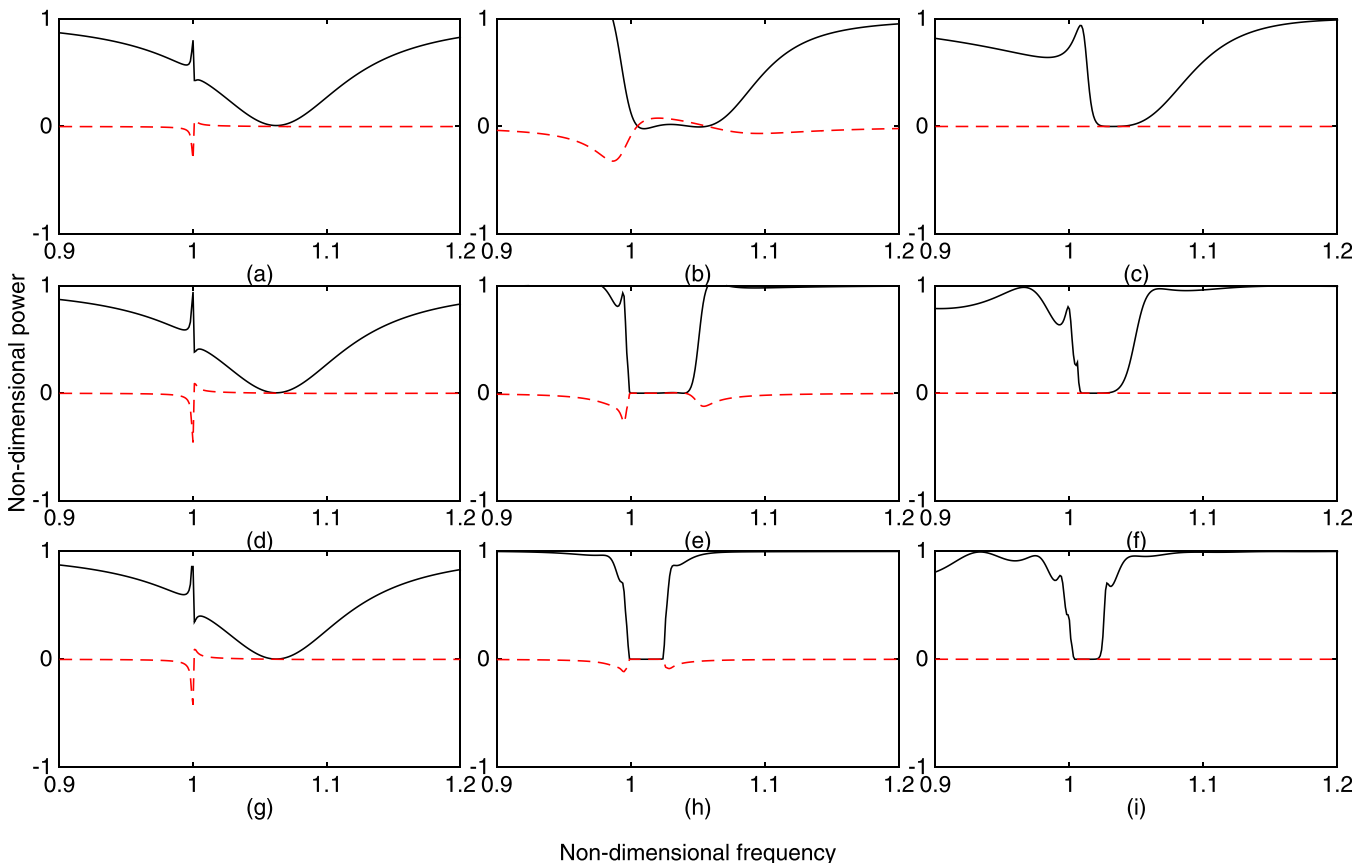

FIG. 15. (Color online) Far field non-dimensional power contributed by the propagating waves, i.e., $|a^+|^2 + |a^-|^2$ in Eq. (A6), ————, and by the evanescent waves, i.e., $2|a_N^+||a_N^-|\sin(\phi_4 - \phi_2)$ in Eq. (A6), - - - - - -, for 2 (row 1), 5 (row 2), and 10 (row 3) resonators in different zones, $k_n l = 0.01$ (column 1), $k_n l = 1$ (column 2), $k_n l = 10$ (column 3).

VI. CONCLUSIONS

Motivated by the local resonance phenomenon and the need for better understanding of periodic structures with local resonators, this work discusses the suppression of bending wave in a beam using multiple resonators with various separation lengths. Through a simple beam model, the power transmission in the beam, the interaction among resonators and the beam, as well as the role played by different wave components, are investigated.

The bending wave suppression effect and the underlying mechanism are shown to depend greatly on the separation length between resonators. This is attributed to the evanescent waves involved in the coupling of the resonators over the beam segment. It is shown that the evanescent waves are responsible for power transmission to the far field in some cases. The fraction of the transmitted power, however, depends on the separation length as well as the number of resonators. More specifically, main conclusions are summarized as follows:

(1) The separation length between resonators is shown to be one of the key parameters affecting the beam-resonator interaction and thus the power transmission. Three zones are identified and demarcated by two threshold values, in terms of non-dimensional separation length $k_n l$.
(2) Zone I ($k_n l < 0.105$) denotes the configuration where resonators are closely spaced. In this case, resonators behave exactly in the same manner as one combined resonator, producing a sharp transmission efficiency dip, attributable to the effective suppression of the propagating wave.
(3) Zone II ($0.105 < k_n l < \pi$) is referred to as the intermediate zone, within which multiple dips can be observed in the power transmission efficiency curve. Within this zone, the interaction between the beam and resonators exhibit complex behavior. Notably, evanescent waves are shown to play an important role in twofold ways: carrying power downstream to the far field through their interaction within the beam segment bounded by the resonators, and reverting power back to the upstream part in the same process. It is, in this region, possible to increase the number of resonators to create a stop band over the frequency region where the resonators are effective.
(4) For larger separation length exceeding half of the bending wavelength (Zone III, $k_n l > \pi$), the influence of the evanescent wave diminishes. The minimum power transmission varies within a bounded region and exhibits periodic pattern, corresponding again to half of the bending wavelength.

APPENDIX

The instantaneous power can be expressed in terms of the beam deformation and the internal force as[22]

$$P(x,t) = -M\dot{\theta} - Qv, \tag{A1}$$

where M, $\dot{\theta}$, Q, and v are, respectively, the bending moment, angular velocity, shear force, and transverse velocity of the beam, respectively, which are related to the transverse displacement w by

$$v = \frac{\partial w}{\partial t}, \quad \dot{\theta} = \frac{\partial^2 w}{\partial x \partial t}, \quad Q = -EI\frac{\partial^3 w}{\partial x^3}, \quad M = EI\frac{\partial^2 w}{\partial x^2}. \tag{A2}$$

Equation (2) can be rewritten in a phasor form as

$$w(x,t) = (|a^+|e^{-jk_b x}e^{i\phi_1} + |a^-|e^{jk_b x}e^{i\phi_2} \\ + |a_N^+|e^{-k_b x}e^{i\phi_3} + |a_N^-|e^{k_b x}e^{i\phi_4})e^{i\omega t}. \tag{A3}$$

Substituting Eq. (A3) into Eq. (A1), the time-averaged power components are derived as

$$\overline{P_m} = \overline{-\text{Re}(M)\text{Re}(\dot{\theta})} = \frac{1}{2}\omega EIk_b^3 \begin{bmatrix} |a^+|^2 - |a^-|^2 + 2|a_N^+||a_N^-|\sin(\phi_4 - \phi_2) \\ +|a^+||a_N^+|e^{-k_b x}[\sin(k_b x - \phi_1 + \phi_2) - \cos(k_b x - \phi_1 + \phi_2)] \\ -|a^+||a_N^-|e^{k_b x}[\cos(k_b x - \phi_1 + \phi_4) + \sin(k_b x - \phi_1 + \phi_4)] \\ -|a^-||a_N^+|e^{-k_b x}[\sin(k_b x - \phi_2 + \phi_3) - \cos(k_b x - \phi_2 + \phi_3)] \\ +|a^-||a_N^-|e^{k_b x}[\sin(k_b x + \phi_3 - \phi_4) + \cos(k_b x - \phi_3 - \phi_4)] \end{bmatrix}, \tag{A4}$$

and

$$\overline{P_s} = \overline{-\text{Re}(Q)\text{Re}(\dot{v})} = \frac{1}{2}\omega EIk_b^3 \begin{bmatrix} |a^+|^2 - |a^-|^2 + 2|a_N^+||a_N^-|\sin(\phi_4 - \phi_2) \\ -|a^+||a_N^+|e^{-k_b x}[\sin(k_b x - \phi_1 + \phi_2) - \cos(k_b x - \phi_1 + \phi_2)] \\ +|a^+||a_N^-|e^{k_b x}[\sin(k_b x - \phi_1 + \phi_4) + \cos(k_b x - \phi_1 + \phi_4)] \\ +|a^-||a_N^+|e^{-k_b x}[\sin(k_b x - \phi_2 + \phi_3) - \cos(k_b x - \phi_2 + \phi_3)] \\ -|a^-||a_N^-|e^{k_b x}[\sin(k_b x + \phi_3 - \phi_4) + \cos(k_b x - \phi_3 - \phi_4)] \end{bmatrix}. \tag{A5}$$

2370   J. Acoust. Soc. Am. **139** (5), May 2016

Cheng Yang and Li Cheng

Summing up Eqs. (A4) and (A5) yields the total time-averaged power in the beam:

$$\bar{P} = \overline{P_m} + \overline{P_s}$$
$$= \omega E I k_b^3 [|a^+|^2 + 2|a_N^+||a_N^-|\sin(\phi_4 - \phi_2) + |a^-|^2].$$
(A6)

It can be seen that, in addition to the power transmitted by a pair of propagating waves, there is a cross-flow term related to the evanescent waves, the amount of which is determined by the displacement magnitudes of the evanescent waves and their phase difference.

[1] Z. Liu, X. Zhang, Y. Mao, Y. Y. Zhu, Z. Yang, C. T. Chan, and P. Sheng, "Locally resonant sonic materials," Science **289**, 1734–1736 (2000).

[2] M. I. Hussein, M. J. Leamy, and M. Ruzzene, "Dynamics of phononic materials and structures: Historical origins, recent progress, and future outlook," Appl. Mech. Rev. **66**, 040802 (2014).

[3] C. C. Claeys, K. Vergote, P. Sas, and W. Desmet, "On the potential of tuned resonators to obtain low-frequency vibrational stop bands in periodic panels," J. Sound Vib. **332**, 1418–1436 (2013).

[4] B. R. Mace, D. Duhamel, M. J. Brennan, and L. Hinke, "Finite element prediction of wave motion in structural waveguides," J. Acoust. Soc. Am. **117**, 2835–2843 (2005).

[5] B. R. Mace and E. Manconi, "Modelling wave propagation in two-dimensional structures using finite element analysis," J. Sound Vib. **318**, 884–902 (2008).

[6] J. M. Renno and B. R. Mace, "On the forced response of waveguides using the wave and finite element method," J. Sound Vib. **329**, 5474–5488 (2010).

[7] Y. Xiao, J. Wen, and X. Wen, "Broadband locally resonant beams containing multiple periodic arrays of attached resonators," Phys. Lett. A **376**, 1384–1390 (2012).

[8] U. Ingard, "On the theory and design of acoustic resonators," J. Acoust. Soc. Am. **25**, 1037–1061 (1953).

[9] J. B. Hunt, *Dynamic Vibration Absorbers* (Mechanical Engineering Publications, Ltd, London, 1980).

[10] F. J. Fahy and C. Schofield, "A note on the interaction between a Helmholtz resonator and an acoustic mode of an enclosure," J. Sound Vib. **72**, 365–378 (1980).

[11] S. J. Estéve and M. E. Johnson, "Reduction of sound transmission into a circular cylindrical shell using distributed vibration absorbers and Helmholtz resonators," J. Acoust. Soc. Am. **112**, 2840–2848 (2002).

[12] D. Li and L. Cheng, "Acoustically coupled model of an enclosure and a Helmholtz resonator array," J. Sound Vib. **305**, 272–288 (2007).

[13] C. Yang, D. Li, and L. Cheng, "Dynamic vibration absorbers for vibration control within a frequency band," J. Sound Vib. **330**, 1582–1598 (2011).

[14] M. J. Brennan, "Control of flexural waves on a beam using a tunable vibration neutralizer," J. Sound Vib. **222**, 389–407 (1999).

[15] H. Salleh and M. J. Brennan, "Control of flexural waves on a beam using a vibration neutraliser: Effects of different attachment configurations," J. Sound Vib. **303**, 501–514 (2007).

[16] H. M. El-Khatib, B. R. Mace, and M. J. Brennan, "Suppression of bending waves in a beam using a tuned vibration absorber," J. Sound Vib. **288**, 1157–1175 (2005).

[17] H. M. El-Khatib, B. R. Mace, and M. J. Brennan, "Wave reflection and transmission in thin beams in the presence of an undamped absorber," ISVR Technical Memorandum 903, University of Southampton, UK (2003).

[18] D. J. Thompson, "A continuous damped vibration absorber to reduce broad-band wave propagation in beams," J. Sound Vib. **311**, 824–842 (2008).

[19] Y. Gao, M. J. Brennan, and F. Sui, "Control of flexural waves on a beam using distributed vibration neutralisers," J. Sound Vib. **330**, 2758–2771 (2011).

[20] F. J. Fahy and P. Gardonio, *Sound and Structural Vibration: Radiation, Transmission and Response*, 2nd ed. (Academic, Amsterdam, 2007), Chap. 1.

[21] L. Cremer, M. Heckl, and B. A. T. Petersson, *Structure-Borne Sound: Structural Vibrations and Sound Radiation at Audio Frequencies*, 3rd ed. (Springer, Berlin, 2005), pp. 245–251.

[22] B. R. Mace, "Wave reflection and transmission in beams," J. Sound Vib. **97**, 237–246 (1984).

J. Acoust. Soc. Am. **139** (5), May 2016

Cheng Yang and Li Cheng   2371